Noise analysis for comparator-based circuits

Noise Analysis for Comparator-Based Circuits

Todd Sepke, *Member, IEEE*, Peter Holloway, Charles G. Sodini, *Fellow, IEEE*, and Hae-Seung Lee, *Fellow, IEEE*

***Abstract*—Noise analysis for comparator-based circuits is presented. The goal is to gain insight into the different sources of noise in these circuits for design purposes. After the general analysis techniques are established, they are applied to different noise sources in the comparator-based switched-capacitor pipeline analog-to-digital converter (ADC). The results show that the noise from the virtual ground threshold detection comparator dominates the overall ADC noise performance. The noise from the charging current can also be significant, depending on the size of the capacitors used, but the contribution was small in the prototype. The other noise sources have contributions comparable to those in op-amp-based designs, and their effects can be managed through appropriate design. In the prototype, folded flicker noise was found to be a significant contributor to the broadband noise because the flicker noise of the comparator extends beyond the Nyquist rate of the converter.**

***Index Terms*—Comparator-based switched-capacitor circuits (CBSCs), comparators, noise analysis, switched-capacitor circuits, zero-crossing-based circuits (ZCBCs).**

I. Introduction

RECENTLY, comparator-based switched-capacitor circuits (CBSCs) [1], [2] and zero-crossing-based circuits (ZCBCs) [3] were proposed as an alternative to traditional operational-amplifier-based circuits. The potential advantages of comparator-based designs depend critically on their noise properties. Therefore, it is important to establish noise analysis methods that provide insight into the different noise sources and their relative contributions. The noise contribution of the threshold detection comparator is a significant factor in determining the accuracy of the signal processing in CBSC. Common frequency domain noise analysis assumes that the amplifier is in steady state, but comparators do not necessarily reach steady state and add noise during their transients. Therefore, the usual assumption of wide-sense-stationary (WSS) noise sources is not always valid.

While a simulation-based approach to the noise analysis of CBSCs has been proposed in [4], this paper describes a set of techniques that are useful for the first-order analysis of noise in threshold comparators and comparator-based systems. These analysis techniques are then applied to a comparator-based switched-capacitor pipeline analog-to-digital converter (ADC) [1], [2]. Section II discusses why nonstationary noise analysis is necessary and how it differs from traditional WSS noise analysis. Section III presents a systematic approach to the nonstationary noise analysis for linear time-invariant (LTI) circuits emphasizing the results for white noise signals. The issues of input-referring noise, noise bandwidth, and noise initial conditions are also addressed. Section III concludes with the nonstationary noise analysis of a transconductance amplifier. In order to handle the analysis of both white and flicker noise sources, Section IV introduces the periodic filtering noise model for sampled data systems that allows for the power spectral density (PSD) analysis of a series of samples using classical noise aliasing concepts [5]–[9]. Section V applies the noise analysis techniques to a previously reported prototype 1.5-bit/stage CBSC pipeline ADC [1], [2]. Section VI compares the measured and predicted noise PSD of the prototype converter. Finally, Section VII summarizes and makes concluding remarks.

Manuscript received March 18, 2007. First published August 04, 2008; current version published March 11, 2009. This work was supported in part by the FCRP Focus Center for Circuit & System Solutions (C2S2) under Contract 2003-CT-888. This paper was recommended by Associate Editor I. Bell.

T. Sepke is with Marvell Semiconductor, Inc., Santa Clara, CA 95054 USA (e-mail: sepketod@alum.mit.edu).

P. Holloway is with National Semiconductor, Salem, NH 03079 USA.

C. G. Sodini and H.-S. Lee are with the Department of Electrical Engineering and Computer Science, Massachusetts Institute of Technology, Cambridge, MA 02139 USA.

Digital Object Identifier 10.1109/TCSI.2008.2002547

II. Background

Traditional noise analysis methods for circuits used in first-order design calculations are based on the assumption of WSS noise signals. This assumption is consistent with the often-used sinusoidal steady-state signal analysis methods where all system transients are ignored. Such analysis techniques cover a broad range of applications in electrical engineering, but many applications rely on transient responses. Well-known techniques exist for analyzing the deterministic signals in these systems such as differential equations, convolution, and Laplace transform methods. Methods for analyzing noise signals in transient systems also exist [10], [11], but these methods are not as widely applied to the first-order analysis of circuit problems.

Two notable exceptions where nonstationary noise behavior has been addressed are the areas of charge transfer or charge sampling devices [12]–[14] and relaxation oscillators [15]. Some of the work on charge transfer devices actually addresses the more complicated case where device parameters are allowed to vary with time [12], [13]. This approach is also appropriate for the dynamic circuits discussed here because of their large signal behavior. However, because the goal is an approximate analysis for design intuition, linear analysis is focused on in this paper. The differential equation analysis presented for the relaxation oscillator jitter calculation in [15] is identical, in principle, to that presented in this paper. The benefit of the approach presented here is that it generalizes to arbitrary LTI systems using the framework of impulse responses and transfer functions [10].

Recently, interest in charge-based sampling circuits [16] that periodically integrate the input signal for a fixed amount of time

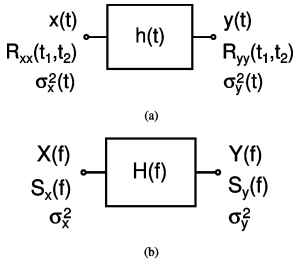

Fig. 1. Overview of time domain and frequency domain analyses. (a) Time domain noise analysis input and output variables. (b) Frequency domain noise analysis input and output variables.

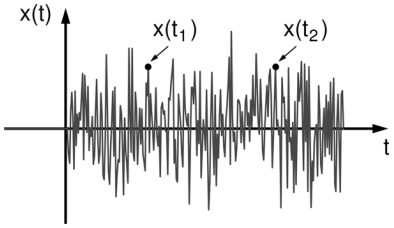

Fig. 2. Step noise signal $\mathbf{x}(t)$. Underlying WSS noise process $\boldsymbol{\nu}(t)$ applied at $t = 0$. If t_1 or t_2 is less than zero, the autocorrelation for $\mathbf{x}(t)$ is zero, and if t_1 and t_2 is greater than zero, the underlying WSS autocorrelation $R_{\nu\nu}(t_1, t_2)$ defines the autocorrelation of $\mathbf{x}(t)$.

has resulted in a series of papers applying this technique for subsampling [14], [17]–[20]. As shown in Section IV, the sampling model and resulting mathematics also apply to the analysis of noise sources in comparator-based systems if the periodic integration is generalized to periodic filtering. Similar mathematical tools have also been employed to analyze phase noise and jitter in CMOS ring oscillators [21].

III. Nonstationary Noise Analysis

Consistent with all other signal analysis problems, noise analysis can be performed in either the time domain or the frequency domain. Fig. 1 shows both the frequency domain and time domain representations of an arbitrary system with input and output variables defined. Although it is possible to analyze nonstationary noise problems in the frequency domain, a time domain analysis is often more natural because the variance of the output noise is a function of time. As a simple example, consider that the step noise input is constructed from an underlying WSS process $\boldsymbol{\nu}(t)$ applied at time zero, as shown in Fig. 2

$$\mathbf{x}(t) = \boldsymbol{\nu}(t)u(t) \tag{1}$$

where $u(t)$ is the unit step function. This is a nonstationary random process because the mean and variance of $\mathbf{x}(t)$ are functions of time. The autocorrelation is then

$$R_{xx}(t_1, t_2) = E\left[\mathbf{x}(t_1)\mathbf{x}(t_2)\right] \tag{2a}$$

$$= R_{\nu\nu}(t_1, t_2)u(t_1)u(t_2) \tag{2b}$$

which is the autocorrelation of the underlying random process when both time points are after the noise input was applied. In order to simplify the nonstationary autocorrelation expressions, it is always assumed that $(t_2 \geq t_1 \geq 0)$.

For nonstationary noise analysis, the usual multiplication in the frequency domain of the input noise PSD by the square of the transfer function is replaced with two convolutions in the time domain of the impulse response with the input noise autocorrelation function

$$R_{yy}(t_1, t_2) = h(t_1) * R_{xx}(t_1, t_2) * h(t_2) \tag{3}$$

where $h(t)$ is the system impulse response. Ultimately, the variance or standard deviation of the output noise amplitude is of interest because the standard deviation can be measured as the rms value of the noise voltage or current. The variance of the output as a function of the autocorrelation is

$$\sigma_y^2(t) = E\left[\mathbf{y}(t)\mathbf{y}(t)\right] = R_{yy}(t_1, t_2)\big|_{t_1=t_2=t}. \tag{4}$$

The special case of a white noise input source is of particular importance because many noise sources can be traced back to white noise generated in circuit components. For a white noise step input, the input autocorrelation is a delta function

$$R_{xx}(t_1, t_2) = \frac{1}{2}S_{xo}\delta(t_2 - t_1) \tag{5}$$

where S_{xo} is the one-sided white noise PSD of the underlying noise process and the delta function means that the noise at different times is uncorrelated. The output variance simplifies to

$$\sigma_y^2(t) = \frac{1}{2}S_{xo}\int_0^t |h(\alpha)|^2 \, \mathrm{d}\alpha. \tag{6}$$

Therefore, to solve for the white noise step response, all that is required is the input white noise PSD and the impulse response from the noise source to the output. A frequency domain interpretation is presented in Section III-E.

A. Time Versus Ensemble Averages

The conventional view of noise voltages and currents in circuit analysis is that they represent the time-averaged rms value of the noise. This interpretation is appropriate for WSS noise processes because the statistics (mean and variance) do not change as a function of time, but for nonstationary noise processes, the statistics, by definition, are a function of time. The time-varying statistics have averages taken over a set (ensemble) of many possible noise waveforms at each instant in time [10]. For example, consider a noisy current source charging a capacitor; the capacitor voltage may look like that shown in Fig. 3. Because the system is linear and superposition applies, the composite waveform can be separated into the average ramp that the dc current causes and a noise voltage that the noise current integrating on the capacitor causes. At any point in time, a statistical distribution describes the possible values of the noise waveform. A time-varying noise variance

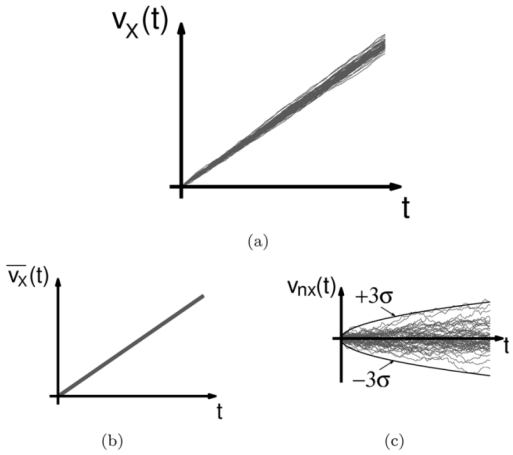

Fig. 3. In transient noise analysis, it is ensemble averages and not time averages that are most important. (a) Ramp voltage plus random walk noise. (b) Average ramp voltage. (c) Random walk noise voltage showing 3σ bounds.

implies that the standard deviation of the voltage distribution is changing with time.

B. Noise Initial Conditions

Another issue with time domain noise analysis is the handling of capacitor and inductor initial conditions due to noise. The nonstationary noise analysis equations given in (3) and (4) determine the noise response for zero initial conditions, also known as the zero-state response. Assuming that the initial conditions are statistically independent of the noise input, the system can be analyzed for zero-state and initial condition responses separately, and their variances add. The assumptions of independent initial conditions should be valid for both white and flicker noise sources. For white noise sources, no correlation exists between noise at different time points, and for flicker noise, nonoverlapping time segments are independent [22], [23].

C. Example: Transconductance Amplifier

As an example of nonstationary noise analysis techniques, the noise and ramp response of a transconductance amplifier representing the first stage of a threshold detection comparator [1], [2] are presented. The equivalent circuit and step ramp input

$$v_{ID} = \left(\frac{\mathrm{d}v_X}{\mathrm{d}t}\right) tu(t) \tag{7}$$

are shown in Fig. 4. The impulse response for the transconductance amplifier is

$$h(t) = \frac{G_m}{C_L} e^{-t/\tau_o} u(t) \tag{8}$$

and the response of this amplifier to the step ramp input (7) is

$$v_{OD}(t) = A_o M \left[t - \tau_o(1 - e^{-t/\tau_o})\right] u(t) \tag{9}$$

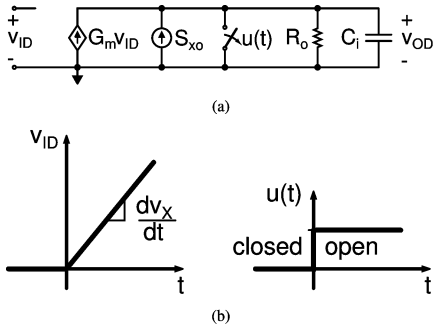

Fig. 4. Half-circuit model for band-limiting preamplifier. (a) Linear half-circuit model. (b) Waveforms for linear half-circuit model.

where $A_o = G_m R_o$ is the dc gain, $\tau_o = R_o C_L$ is the amplifier time constant, and $M = \mathrm{d}v_X/\mathrm{d}t$ is the input ramp rate. The impulse response from the noise current source to the output voltage is

$$h_n(t) = \frac{1}{C_L} e^{-t/\tau_o} u(t). \tag{10}$$

Substituting (10) into (6) and modeling the noise current PSD $S_{xo} = 4kTG_n$ as the thermal noise from an equivalent noise conductance G_n, the noise at the output of the amplifier is

$$\overline{v_{\mathrm{on}}^2}(t) = \left(\frac{G_n}{G_m}\right) \frac{kT}{C_L} (G_m R_o)[1 - e^{-2t/\tau_o}] u(t). \tag{11}$$

This result simplifies into two interesting special cases

$$\overline{v_{\mathrm{on}}^2}(t) = \begin{cases} \left(\frac{G_n}{G_m}\right) \frac{kT}{C_L} (G_m R_o), & t \gg \tau_o/2 \quad \text{(12a)} \\ \frac{2kTG_n}{C_L^2} t, & t \ll \tau_o/2 \quad \text{(12b)} \end{cases}$$

where (12a) is the usual steady-state noise result for a broadband amplifier, and (12b) is a random walk [10] resulting from integrating a white noise current onto the load capacitance C_L for an ideal transconductance amplifier.

In order to input-refer the output noise voltage, the noise gain of the amplifier must be calculated. Modeling a finite-bandwidth threshold detection comparator as a cascade of an amplifier and an ideal threshold comparator, the output noise voltage of the amplifier results in jitter of the output threshold crossing through the rate of change of the amplifier output voltage, as shown in Fig. 5(a). To refer the output voltage noise to the input of the amplifier, it is desired to have an input noise voltage that results in the same comparator jitter when the input voltage crosses the input threshold voltage V_{CM}, as shown in Fig. 5(b).

The conversion of noise voltages to timing jitter happens when a threshold detection device senses a noisy signal [24]. To see how this occurs, consider Figs. 5 and 6. The signal crosses the threshold at the output of the preamplifier V_{Mo} at some average rate $\overline{\mathrm{d}v_{OD}/\mathrm{d}t}$ and has a noise voltage distribution at the average crossing time t_i, as shown on the right of Fig. 6. Assuming that the noise voltage variations are small over the range of possible crossing times, the standard deviation of the

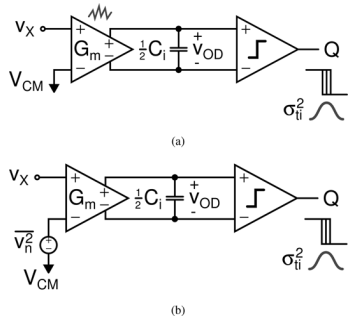

Fig. 5. Input-referred noise modeling. (a) Noisy preamplifier results in threshold comparator jitter at output threshold crossing. (b) Noiseless preamplifier with input-referred noise voltage ($\overline{v_n^2}$ in V^2) results in the same jitter at the input threshold crossing.

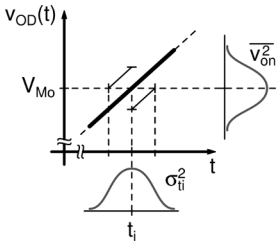

Fig. 6. Transformation of voltage noise to timing jitter in the comparator decision.

noise voltage projects back to the threshold with the average slope

$$\sigma_{ti}^2 = \overline{v_{\rm on}^2}\left|\frac{{\rm d}v_{OD}}{{\rm d}t}\right|_{v_{OD}=V_{Mo}}^{-2} \tag{13}$$

which defines the variance of a distribution of times that the threshold is crossed. The variation in time is the jitter in the threshold crossing time. For an input-referred noise voltage $\overline{v_n^2}$, the jitter calculated at the input is

$$\sigma_{ti}^2 = \overline{v_n^2}\left|\frac{{\rm d}v_X}{{\rm d}t}\right|_{v_X=V_{CM}}^{-2} \tag{14}$$

where V_{CM} is the threshold at the input of the amplifier. Setting the jitter from the output noise equal to the jitter from the input-referred noise so that the models in Fig. 5 result in the same jitter, the input-referred noise is

$$\overline{v_n^2} = \frac{\overline{v_{\rm on}^2}}{|A_N|^2} \tag{15}$$

where the noise gain is

$$|A_N| = \left(\left|\frac{{\rm d}v_{OD}}{{\rm d}t}\right|_{v_O=V_{Mo}}\right) \Big/ \left(\left|\frac{{\rm d}v_X}{{\rm d}t}\right|_{v_X=V_{CM}}\right) \tag{16}$$

and is a function of the response time t_i of the amplifier. Note that slew rate limitations in the preamplifier place a practical upper limit on the noise gain for a given bias current. Using this definition of noise gain for the amplifier in Fig. 4 with a ramp input, the noise gain is

$$|A_N(t_i)| = A_o(1 - e^{-t_i/\tau_o})u(t_i) \tag{17}$$

which approaches the small-signal gain if the amplifier reaches steady state during the response time ($t_i \gg \tau_o$). Dividing the output mean-squared noise voltage (11) by the noise-gain-squared $|A_N(t_i)|^2$ results in the mean-squared input-referred noise voltage of the amplifier

$$\overline{v_n^2}(t_i) = 4kTR_n\frac{1}{4\tau_o}\coth\left(\frac{t_i}{2\tau_o}\right)u(t_i) \tag{18}$$

where $4kTR_n$ is recognized as the usual input-referred noise PSD of the transconductance amplifier $R_n = G_n/G_m^2$, and the rest of the expression is the effective noise bandwidth.

D. Effective Noise Bandwidth

It is interesting to note that the noise bandwidth of the input-referred noise in (18) is similar to the usual one-pole system noise bandwidth

$$NBW = \frac{\pi}{2}f_{3\,\rm dB} = \frac{1}{4\tau_o} \tag{19}$$

where $f_{3\,\rm dB} = (2\pi\tau_o)^{-1}$ is the 3-dB bandwidth of the amplifier. The nonstationary effective noise bandwidth for the transconductance amplifier is

$$NBW(t_i) = \frac{1}{4\tau_o}\coth\left(\frac{t_i}{2\tau_o}\right)u(t_i) \tag{20}$$

and the following two limits are of interest:

$$NBW(t_i) = \begin{cases} \frac{1}{4\tau_o}, & t_i \gg \tau_o/2 \quad (21a) \\ \frac{1}{2t_i}, & t_i \ll \tau_o/2 \quad (21b) \end{cases}$$

where (21a) is the WSS noise bandwidth and (21b) is the noise bandwidth for an ideal integrator or transconductance amplifier. A plot of the generalized noise bandwidth, including asymptotic limits, is shown in Fig. 7. For a given response time t_i, the noise bandwidth asymptotically approaches its minimum value $1/(2t_i)$ as the amplifier time constant τ_o approaches infinity. Therefore, for a given transconductance and load capacitance, an ideal transconductance amplifier with infinite time constant is not only fastest to reach a threshold from a reset condition [25] but also has the lowest noise bandwidth and input-referred noise voltage [26].

E. Frequency Domain Interpretation

The generalized definition of noise bandwidth presented earlier suggests a frequency domain interpretation of the nonstationary noise problem for step white noise inputs. The integral in (6) can be rewritten as

$$\sigma_y^2(t) = \frac{1}{2}S_{xo}\int_{-\infty}^{+\infty}|h_w(\alpha)|^2\,{\rm d}\alpha \tag{22}$$

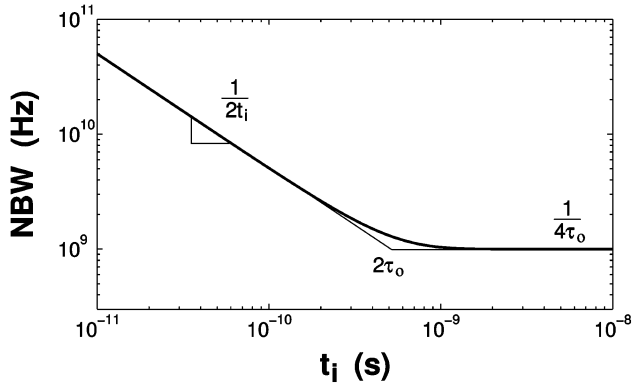

Fig. 7. Noise bandwidth versus response time t_i, $\tau_o = 250$ ps.

where

$$h_w(t) = w(t)h(t) \tag{23}$$

$h(t)$ is the system impulse response, and $w(t)$ is a rectangular window function of unit amplitude from time zero to time t_i and zero otherwise. Using Parseval's theorem

$$\sigma_y^2(t) = \frac{1}{2} S_{xo} \int_{-\infty}^{+\infty} |H_w(f)|^2 \, \mathrm{d}f \tag{24}$$

where the Fourier transform $H_w(f)$ of the windowed impulse response $h_w(t)$ is the transfer function from the noise source to the output. Given the transfer function $H_w(f)$, the effective noise bandwidth can be defined as the equivalent brick wall filter in the usual manner

$$NBW(t) = \frac{1}{|H_w(0)|^2} \int_{0}^{+\infty} |H_w(f)|^2 \, \mathrm{d}f \tag{25}$$

where $\sigma_y^2(t) = |H_w(0)|^2 S_{xo} NBW(t)$. However, this frequency domain interpretation only applies to the nonstationary noise analysis of white noise inputs due to the assumption of a white noise autocorrelation in deriving (6) from the more general relationships in (3) and (4).

IV. Periodic Filtering Frequency Domain Model

Nonstationary noise analysis is useful for understanding the circuit response to a step noise input as a function of the response time t_i, but sampled data systems operate on the series of discrete-time samples taken at the end of the sampling period. Therefore, it is the statistics of the series of samples that are of interest. Although the details of the processing during each period result in nonstationary noise voltages and currents, the same operation is performed each clock cycle, resulting in the same signal statistics each clock cycle. This means that the process is wide-sense cyclostationary. The periodically sampled values then all have the same statistics and form a WSS discrete-time series. To analyze this discrete-time series of samples, a periodic filtering model is presented as an extension of the periodic integration model in [14]. Because the periodic filtering model examines a sequence of samples in time, it is suitable for the analysis of both white and flicker noise sources. First, the periodic filtering sampler model is described, and the filter transfer function is defined. Then, well-known noise aliasing techniques [5]–[9] can be applied to obtain a noise PSD estimate for the series of samples.

The derivation for the model of a periodic filtering sampler is an extension of that presented in [14] for a periodic integrating sampler to an arbitrary filtering function. The value of the nth sample of the output $y(t)$ for a system that integrates the input $x(t)$ from time nT_s to $nT_s + t_i$ is

$$y(nT_s + t_i) = \int_{nT_s}^{nT_s + t_i} x(\tau) \, \mathrm{d}\tau \tag{26}$$

$$= \int_{-\infty}^{+\infty} x(\tau) w(nT_s + t_i - \tau) \, \mathrm{d}\tau \tag{27}$$

where $w(t)$ is the rectangular window function of unit height and duration t_i. Realizing that the second integral is the convolution of the input $x(t)$ to a time-shifted impulse response of a finite-duration integrator $w(t)$, the procedure is easily extended to finite-duration filtering of an arbitrary impulse response

$$y(nT_s + t_i) = \int_{-\infty}^{+\infty} x(\tau) h_w(nT_s + t_i - \tau) \, \mathrm{d}\tau \tag{28}$$

where $h_w(t)$ is the windowed impulse response (23). It should be noted that it is the zero-state response that is found from the convolution of the input with an impulse response. Therefore, this procedure assumes that the output is reset between operations. Because the noise from the reset can be treated as an independent random initial condition, the total noise is the superposition of the initial condition (zero-input) response and the zero-state response. Continuing with the model derivation, the series of periodically filtered samples can be expressed as the infinite sum of samples

$$\sum_{n=-\infty}^{+\infty} y(nT_s + t_i) \delta(t - nT_s - t_i) = y(t) \delta_{T_s}(t - t_i) \tag{29}$$

which is the impulse train sampling of the output, where the usual shorthand notation for the sampling impulse train

$$\delta_{T_s}(t) = \sum_{n=-\infty}^{+\infty} \delta(t - nT_s) \tag{30}$$

has been used. The output samples of the periodic filtering system can be modeled, as shown in Fig. 8, according to

$$y(t) \delta_{T_s}(t - t_i) = [x(t) * h_w(t)] \, \delta_{T_s}(t - t_i) \tag{31}$$

where $h_w(t)$ is the windowed impulse response of the system. The model in Fig. 8 reduces to that originally suggested in

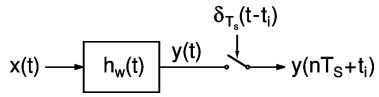

Fig. 8. Periodic filtering sampler model: The output samples can be modeled as the impulse train sampling of the input filtered by the Fourier transform of the windowed impulse response.

[16] and used in [18] and [19] for a periodic integrating system $h_w(t) = w(t)$.

To apply the periodic filtering model to existing noise aliasing techniques, the frequency domain transfer function from the noise source to the output $H_w(f) = \mathcal{F}\{h_w(t)\}$ is more useful. The procedure for determining the filter transfer function is to find the Laplace s-domain transfer function from the noise source to the output. The inverse Laplace transfer yields the system impulse response $h(t)$. The Fourier transform of the windowed impulse response $h_w(t) = h(t)w(t)$ produces the desired filter function. Summarizing mathematically

$$h(t) = \mathcal{L}^{-1}\{H(s)\} \tag{32a}$$

$$H_w(f) = \mathcal{F}\{h_w(t)\}. \tag{32b}$$

The one-sided noise PSD of the sampled output can then be found from the sum of the filtered and shifted two-sided input noise PSD S_{xx}[5]–[8], [10]

$$S_y(f) = \sum_{n=-\infty}^{+\infty} |H_w(f - nf_s)|^2 \, 2S_{xx}(f - nf_s) \tag{33}$$

which is valid over the Nyquist range $(0 \le f \le f_s/2)$. For numerical calculations, the limits of summation can be truncated to a finite value from knowledge of the effective noise bandwidth of $H_w(f)$[6].

V. CBSC Prototype Pipeline ADC

Recently, a comparator-based switched-capacitor (CBSC) technique was presented that uses comparators to detect virtual ground conditions instead of forcing them with op-amps [1], [2]. The basic architecture of the prototype pipeline ADC is reviewed, and an expression for the total input-referred noise of the ADC is derived in terms of the contribution of a single pipeline stage. The noise contributors to a pipeline stage are then identified, and the noise analysis techniques presented earlier are used to derive the periodic filtering transfer functions to calculate the input-referred noise PSD of the converter.

A. 1.5-bit/Stage CBSC Pipeline ADC

A simplified schematic of the first two stages of the prototype pipeline ADC is shown in Fig. 9. For the prototype, a single-ended circuit design was used, as shown in the schematic. The charge transfer phase operates in two subphases, i.e., coarse (I_1) and fine (I_2). For the purposes of analyzing the input-referred noise of the ADC, the pipeline can be modeled as an input sample-and-hold and a cascade of gain-of-two amplification stages that each resolves 1.5 effective bits, as shown in Fig. 10 [27], [28].

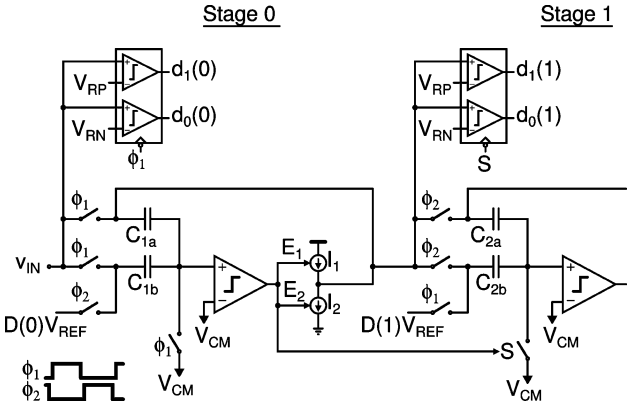

Fig. 9. First two stages of pipeline ADC. Note that the first-stage sampling and bit-decision clocking are controlled by the system clock, but for the second and subsequent stages, the sampling and bit-decision clocking are controlled by the comparator of the previous stage.

Measurements of the output codes for a dc input signal to the ADC can be used to obtain an input-referred noise PSD estimate for the ADC including quantization noise. Because the prototype pipeline was implemented as a cascade of identical stages, the total input-referred noise from the residue amplifiers has a particularly simple form. Referring to Fig. 10, the input-referred noise PSD of an N-bit ADC due to noise in the residue calculations is

$$S_{n,\mathrm{ADC}}(f) = \frac{4}{3}\left[1 - \left(\frac{1}{4}\right)^{N-1}\right] S_{n0}(f) \tag{34}$$

$$\approx \frac{4}{3} S_{n0}(f) \tag{35}$$

where $S_{n0}(f)$ is the input-referred noise PSD of a single stage, and the final approximation in (35) is true for a large number of bits $(N \gg 1)$ and converges quickly [26]. The kT/C noise of the input sampler and the ADC quantization noise add to the input-referred noise PSD to give the total input noise PSD. In total

$$S_{n,\mathrm{total}}(f) = S_{\mathrm{sample}}(f) + S_{n,\mathrm{ADC}}(f) + S_q(f) \tag{36}$$

where $S_{\mathrm{sample}}(f) = kT/C_s/(f_s/2)$ is the noise PSD from the input sampler over the Nyquist range and $S_q(f) = V_{\mathrm{LSB}}^2/12/(f_s/2)$ is the ADC quantization noise.

B. Input-Referred Noise of a Single Pipeline Stage

The input-referred noise of a single stage has three components, namely, noise from the comparator decision, noise from the switches, and noise from the fine-phase charging current source I_2 in Fig. 9. Transfer functions from each of these noise sources referred to the input of the pipeline stage are derived for use in the periodic filtering model that was described in Section IV. Results for the special case of white noise sources are summarized for the optimum case of an ideal transconductance preamplifier $(t_i \ll \tau_o/2)$.

1) Threshold Detection Comparator Noise: The simplified schematic of the threshold detection comparator with a band-limiting preamplifier is shown in Fig. 5, and a transistor-level

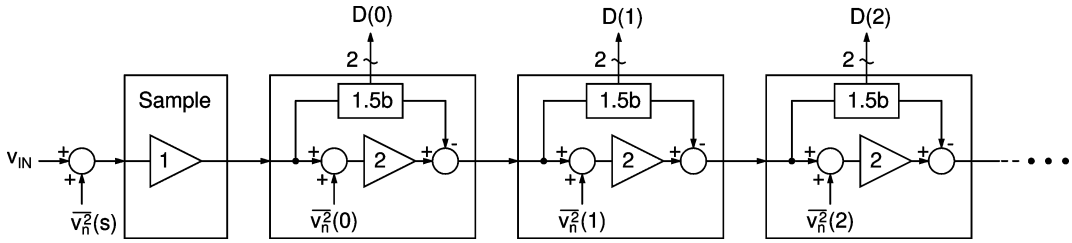

Fig. 10. Pipeline ADC model that resolves 1.5 b/stage. The noise added at each stage contributes to uncertainty in the output residue voltage of the stage.

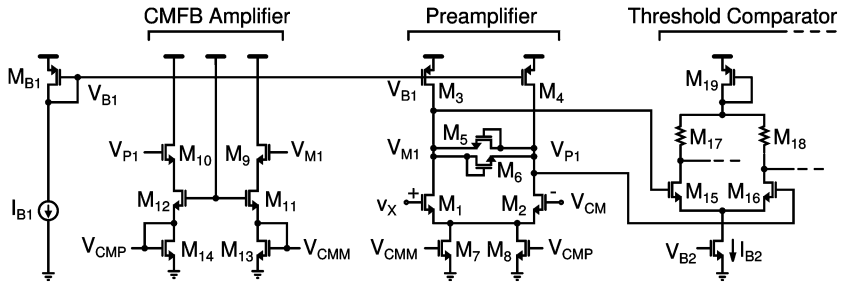

Fig. 11. Schematic of preamplifier for the comparator used in the prototype [1], [2].

schematic of the preamplifier used in the prototype [1], [2] is shown in Fig. 11, with output signals shown in Fig. 12. The circuit implements the function of the transconductance amplifier and the threshold comparator in Fig. 5. The band-limiting capacitor $C_i/2$ is not explicit in Fig. 11 but consists of parasitic capacitance at the output of the preamplifier. Noise in the coarse charge transfer phase decision only causes variation in the duration of the charge transfer time and does not affect the accuracy of the sampled value. It is the noise in the fine charge transfer phase decision that determines the accuracy of the sampled value. After the coarse-phase decision, the output of the preamplifier is assumed to be clamped so that $(1/2)C_i$ has $-V_D$ across it. When the voltage on the output capacitance is clamped, it does not begin to discharge during the fine charge transfer phase until the differential input voltage to the transconductance preamplifier is greater than the input-referred clamp voltage ($|v_{ID}| > |V_D|/A_o$). An approximate linear half-circuit model for the preamplifier that neglects slew rate limitations is shown in Fig. 4(a) where its differential input voltage is modeled as a step ramp waveform and the noise from the transconductance device starts charging the output capacitance at time zero [Fig. 4(b)]. The noise from the preamplifier consists of the clamp state noise contribution and the noise current added to the band-limiting capacitance during the response time t_i, as defined in Fig. 12.

The noise from the clamped state is a noise initial condition on the band-limiting capacitance ($(1/2)C_i$). The noise from the clamp device (M_5 or M_6) and the noise from the current passing through the clamp from M_3 or M_4 feed noise to the band-limiting capacitor. The transfer function from these two noise sources to the output is the low-pass filter at the output of the preamplifier in the clamp state

$$|H_{\text{clamp}}(f)|^2 = \frac{1/G_D^2}{1+(2\pi f\tau_c)^2} \tag{37}$$

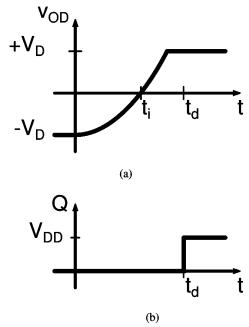

Fig. 12. Ideal timing for comparator with preamplifier. The preamplifier output voltage is clamped at $\pm V_D$. (a) Preamplifier output voltage showing the response time t_i that it takes for the preamplifier output to reach the comparator threshold. (b) Output logic signal changes state after total comparator delay t_d.

where the preamplifier time constant in the clamp state is $\tau_c = (1/2)C_i/G_D$ and G_D is the on conductance of the diode-connected device. During the preamplifier response time t_i, the preamplifier time constant $\tau_o = R_oC_i$ determines the rate at which the initial condition decays and the noise gain increases

$$|H_{w,ic}(f)|^2 = \frac{e^{-2t_i/\tau_o}}{|A_N(t_i)|^2} \tag{38}$$

where $|A_N(t_i)|$ is the preamplifier noise gain (17). The periodic filtering transfer function from noise in the clamp state referred to the input of the gain stage can then be expressed as the product of these two transfer functions

$$|H_{w,\text{clamp}}(f)|^2 = |H_{\text{clamp}}(f)|^2\,|H_{w,ic}(f)|^2\,. \tag{39}$$

If the time constant during the preamplifier response time is much greater than the response time ($t_i \ll \tau_o/2$), then the

clamp noise is just input-referred by the preamplifier noise gain $|A_n(t_i)|^2$.

Assuming that the preamplifier is an ideal transconductance amplifier ($t_i \ll \tau_o/2$) and modeling the white noise from the current source and diode clamp devices as an equivalent thermal noise $4kTG_{nD}$ that is sampled onto the integration capacitor $(1/2)C_i$ when the clamp device turns off, the input-referred clamp noise is

$$\overline{v_{n,\text{clamp}}^2} = 2\left(\frac{G_{nD}}{G_D}\right)\left(\frac{kT}{C_i}\right)\frac{1}{|A_N(t_i)|^2} \tag{40}$$

where the noise gain (17) of an ideal transconductance amplifier is

$$|A_N(t_i)| = \frac{G_m}{C_i}t_i. \tag{41}$$

Therefore, for a large noise gain, the preamplifier needs to be fast (large G_m/C_i) and have a large steady-state gain (large R_o). The relative importance of the clamp noise is discussed after the analysis of the noise contribution during the preamplifier response time.

During the preamplifier response time, the noise current from the transconductance amplifier adds noise to the output voltage of the preamplifier. Using (32), the general transfer function from the output noise current of the transconductance amplifier referred to the input of the gain stage is

$$|H_{w,\text{resp}}(f)|^2 = \left(\frac{1/G_m^2}{1+(2\pi f\tau_o)^2}\right)|H_{w,t_i}(f)|^2 \tag{42}$$

where the first portion is the steady-state transfer function and the response time portion of the transfer function

$$|H_{w,t_i}(f)|^2 = \frac{1-2e^{-t_i/\tau_o}\cos(2\pi f t_i)+e^{-2t_i/\tau_o}}{1-2e^{-t_i/\tau_o}+e^{-2t_i/\tau_o}}. \tag{43}$$

The preamplifier noise simplifies into two interesting special cases for a broadband preamplifier and an ideal transconductance preamplifier

$$|H_{w,\text{resp}}(f)|^2 = \begin{cases} \frac{1/G_m^2}{1+(2\pi f\tau_o)^2}, & t_i \gg \tau_o/2 \quad \text{(44a)} \\ \frac{1}{G_m^2}\text{sinc}^2(ft_i), & t_i \ll \tau_o/2. \quad \text{(44b)} \end{cases}$$

For the broadband case (44a), the transfer function simplifies to the expected steady-state result which is independent of the response time t_i and has a constant noise bandwidth. For the case of an ideal transconductance preamplifier (44b), the transfer function simplifies to a sinc function. Using (25), it can be shown that the effective noise bandwidth of the sinc transfer function is inversely proportional to the response time. These two results are identical to the effective noise bandwidths for white noise sources (21a) and (21b) described in Section III. A plot of the transfer function $|H_{w,\text{resp}}(f)|$ versus frequency for three different response times is shown in Fig. 13.

Assuming only thermal noise contributions from an ideal transconductance preamplifier ($t_i \ll \tau_o/2$), the input-referred noise contribution is

$$\overline{v_{n,\text{resp}}^2} = 4kT\left(\frac{G_n}{G_m^2}\right)\frac{1}{2t_i} \tag{45}$$

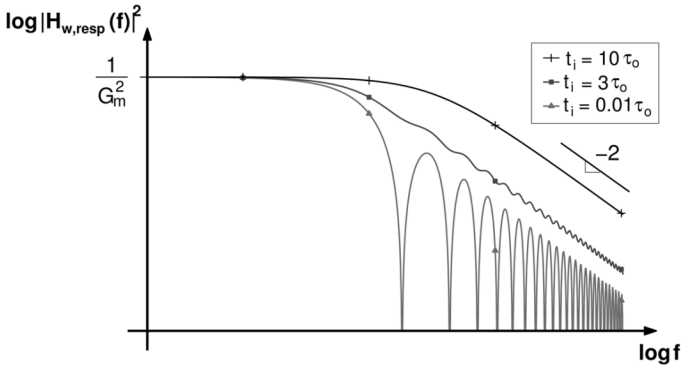

Fig. 13. Preamplifier response time filter $|H_{w,\text{resp}}(f)|^2$ for different output resistances causing variation in t_i relative to $\tau_o/2$.

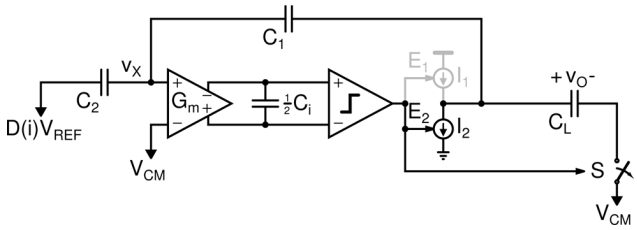

Fig. 14. Noise contribution from fine-phase charging current I_2.

where the dc gain is taken from (44b) and the noise bandwidth of $\text{sinc}(ft_i)$ is $1/2t_i$. To compare the response noise with the clamp state noise, (45) can be rewritten as

$$\overline{v_{n,\text{resp}}^2} = 2\left(\frac{G_n}{G_m}\right)\left(\frac{kT}{C_i}\right)\frac{1}{|A_N(t_i)|} \tag{46}$$

using the ideal transconductance amplifier noise gain (41). The total input-referred noise for the preamplifier is then the sum of (40) and (46)

$$\overline{v_{n,\text{preamp}}^2} = \overline{v_{n,\text{resp}}^2}\left[1+\left(\frac{G_m}{G_n}\right)\left(\frac{G_{nD}}{G_D}\right)\frac{1}{|A_N(t_i)|}\right]. \tag{47}$$

If the preamplifier noise gain is relatively large

$$|A_N(t_i)| \gg \left(\frac{G_m}{G_n}\right)\left(\frac{G_{nD}}{G_D}\right) \tag{48}$$

the preamplifier noise dominates.

The noise contribution of the comparator is similar to that of the op-amp in an op-amp-based design. From (45), a potential advantage of comparator-based designs is apparent in the noise bandwidth that is a function of the preamplifier integration time. Assuming that t_i can be made longer than the required time constant in an op-amp-based system, the noise from the comparator is lower than that of the op-amp for the same power [2].

2) Charging Current Noise: The second source of noise to be considered during the charge transfer phase is the contribution from the fine-phase charging current source I_2 shown in Fig. 14. The noise from the charging current I_2 only adds noise to the

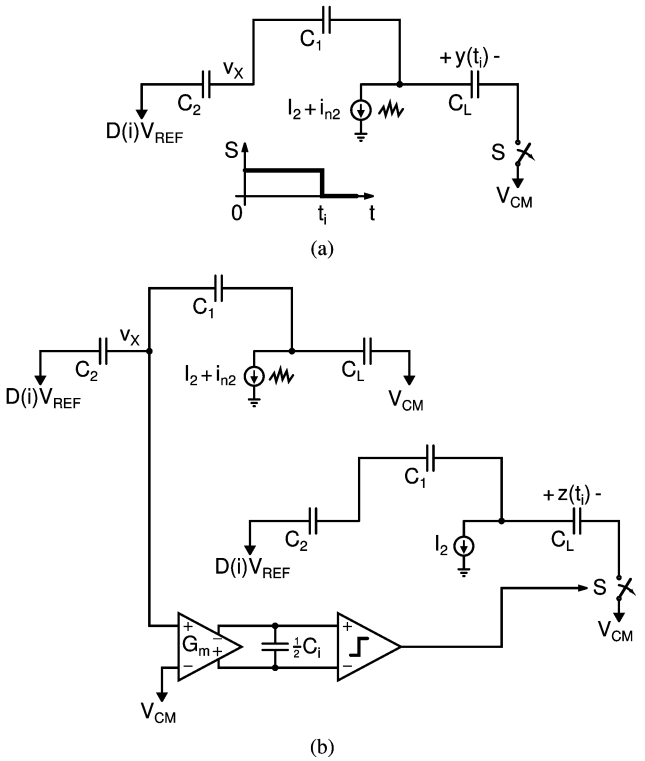

Fig. 15. Charging current noise analysis with correlated sampling jitter. (a) Open-loop random walk noise voltage $y(t_i)$ on C_L after response time t_i. (b) Noise voltage $z(t_i)$ sampled on C_L due to jitter in comparator decision only.

sampled output value after the preamplifier input threshold is crossed. The noise added to the capacitor network before this time does not effect the final value and only changes the time that it takes to reach the preamplifier input threshold. The noise contribution from the charging current consists of the random walk deviation on the external capacitor network during two independent time intervals. The first interval is the preamplifier response time t_i from Fig. 12, and the second interval is the delay time from the threshold detection to the sampling switch opening $t_d - t_i$.

The preamplifier filters the random walk on the capacitor network during the preamplifier response time and results in a jitter in the comparator decision. This jitter is negatively correlated with the random walk deviation during the preamplifier response time and partially cancels the sampled random walk deviation. For example, consider a larger than average random walk deviation at the preamplifier input. This larger than average deviation results in a larger than average preamplifier output and a shorter than average time to reach the comparator threshold voltage. Therefore, the shorter than average comparator delay partially cancels the larger than average random walk deviation.

To derive the periodic filtering transfer function for the charging current noise that accounts for the cancellation due to the negatively correlated jitter, consider the open-loop random walk deviation at the output $y(t_i)$ in Fig. 15(a) and the sampled noise voltage at the output due only to the sampling jitter $z(t_i)$ in Fig. 15(b) separately. The total noise voltage on the sampled output is the difference between these two voltages $v_o(t_i) = y(t_i) - z(t_i)$.

Referring to Fig. 15(a), the open-loop random walk deviation is calculated assuming that the sampling instant is independent of the random walk deviation. Under this assumption, the s-domain transfer function from the charging current noise directly to the output voltage is

$$H_y(s) = \frac{1}{sC_E} \tag{49}$$

where $C_E = C_L + C_x$ is the total capacitance at the output of the gain stage, with C_x being the series combination of C_1 and C_2.

The sampled noise voltage at the output due only to jitter in the comparator decision can be calculated using the circuit in Fig. 15(b). The circuit consists of a noisy current source charging the copy of the capacitor network that the comparator senses, and the comparator opens the sampling switch in a noiseless copy of the capacitor network. For this circuit, the s-domain transfer function from the charging current noise to the sampled output voltage is

$$\begin{aligned} H_z(s) &= \left(\frac{1}{sC_E}\right)\left(\frac{C_1}{C_1+C_2}\right)\left(\frac{A_o}{1+s\tau_o}\right)\frac{|\mathrm{d}z/\mathrm{d}t|}{|\mathrm{d}v_{OD}/\mathrm{d}t|} \\ &= \left(\frac{1}{sC_E}\right)\left(\frac{A_o}{1+s\tau_o}\right)\frac{1}{|A_N(t_i)|} \end{aligned} \tag{50}$$

where the transformations from noise voltage to jitter and jitter to sampled noise voltage are accomplished with the rate at which the preamplifier output crosses the comparator threshold $|\mathrm{d}v_{OD}/\mathrm{d}t|$ and the ramp rate on the load capacitance $|\mathrm{d}z/\mathrm{d}t|$, respectively. The second equality follows from (16) and

$$\left|\frac{\mathrm{d}v_X}{\mathrm{d}t}\right| = \left(\frac{C_1}{C_1+C_2}\right)\left|\frac{\mathrm{d}z}{\mathrm{d}t}\right| \tag{51}$$

where $|\mathrm{d}z/\mathrm{d}t|$ is related to $|\mathrm{d}v_X/\mathrm{d}t|$ because the average ramp rates are the same in both copies of the circuit in Fig. 15(b).

The s-domain transfer function from the charging current noise to the sampled output voltage noise referred to the input of the gain stage is

$$H_{I_2}(s) = \frac{C_1}{C_1+C_2}\left[H_y(s) - H_z(s)\right]. \tag{52}$$

The periodic filtering transfer function $H_{w,I_2}(f)$ can be obtained using the sequence of transforms described in (32).

To understand the properties of this transfer function, the limiting cases of a wide-bandwidth preamplifier ($t_i \gg \tau_o/2$) and an ideal integrator for a preamplifier ($t_i \ll \tau_o/2$) are considered. The dc gain and noise bandwidth of the transfer function are

$$|H_{w,I_2}(0)|^2 = \begin{cases} \frac{\tau_o^2}{C_E^2}\left(\frac{C_1}{C_1+C_2}\right)^2, & t_i \gg \tau_o/2 \quad (53a) \\ \frac{1}{4}\frac{t_i^2}{C_E^2}\left(\frac{C_1}{C_1+C_2}\right)^2, & t_i \ll \tau_o/2 \quad (53b) \end{cases}$$

$$NBW_{w,I_2} = \begin{cases} \frac{1}{4\tau_o}, & t_i \gg \tau_o/2 \quad (54a) \\ \frac{2}{3t_i}, & t_i \ll \tau_o/2. \quad (54b) \end{cases}$$

Plots of the transfer function $H_{w,I_2}(f)$ are shown for three values of preamplifier response time t_i in Fig. 16.

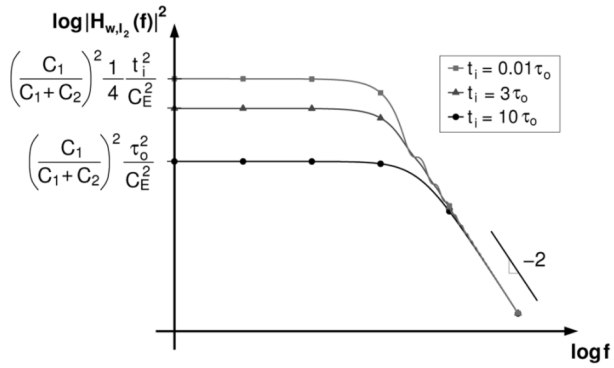

Fig. 16. Charging current transfer function $H_{w,I_2}(f)$ during preamplifier response time for different preamplifier output resistances causing variation in t_i relative to $\tau_o/2$. A broadband preamplifier ($t_i \gg \tau_o/2$) results in more noise cancellation and lower transfer function gain.

For a wide-bandwidth preamplifier ($t_i \gg \tau_o/2$), the noise at the output of the preamplifier is proportional to the noise at the input of the preamplifier at low frequencies. For an infinite-bandwidth preamplifier, they would be proportional at all frequencies, and the jitter would completely cancel the open-loop random walk deviation because it has a correlation coefficient of $c_{yz} = -1$. For a finite bandwidth, higher frequencies have a phase delay resulting in less than complete cancellation. This behavior is also seen in the expressions for dc gain and NBW, (53a) and (54a), respectively. The noise bandwidth increases proportionally to the increase in preamplifier bandwidth (decrease in τ_o), but the magnitude of the dc gain squared is decreasing with the bandwidth squared. For white noise, the rms sampled noise voltage decreases with increasing preamplifier bandwidth (decreasing τ_o).

In the other extreme, an ideal transconductance preamplifier ($t_i \ll \tau_o/2$) has a correlated jitter, but its correlation is approaching its minimum. Using the transfer functions $H_y(s)$ and $H_z(s)$, it can be shown using techniques for correlated noise sources [10] that the correlation coefficient for white noise in the charging current source and an ideal transconductance preamplifier is $c_{yz} = -\sqrt{3}/2$. The decrease in correlation is evident in the expressions for dc gain and NBW, (53b) and (54b), respectively. For a given preamplifier response time t_i, the product of the dc gain squared and the NBW has reached a maximum value versus decreasing preamplifier bandwidth (increasing τ_o).

Assuming that the charging current source I_2 has shot noise $2qI_2$ and that the preamplifier is an ideal transconductance amplifier, multiplying (53b) and (54b) and $2qI_2$ gives the input-referred noise contribution from I_2

$$\overline{v_{n,I_2}^2} = \frac{1}{3}\left(\frac{qI_2}{C_E^2}t_i\right)\left(\frac{C_1}{C_1+C_2}\right)^2. \tag{55}$$

This result is recognized as the input-referred random walk noise multiplied by the 1/3 factor, which is due to the noise cancellation from the negatively correlated jitter.

After the output of the preamplifier trips the threshold comparator, the charging current noise accumulates on the external capacitor network until the output sampling switch is opened. The s-domain transfer function for the input-referred noise contribution is

$$H_{w,I_{2c}}(s) = \frac{1}{sC_E}\left(\frac{C_1}{C_1+C_2}\right)^2. \tag{56}$$

Therefore, the noise transfer function is

$$|H_{w,I_{2c}}(f)|^2 = \left(\frac{t_c}{C_E}\right)^2\left(\frac{C_1}{C_1+C_2}\right)^2 \operatorname{sinc}^2(ft_c) \tag{57}$$

where $t_c = t_d - t_i$ is the threshold comparator delay.

The relative importance of the noise contributions during the preamplifier response time t_i and the threshold comparator delay time t_c depends on the bandwidth of the preamplifier and the length of the comparator delay time versus the preamplifier response time. Again, assuming white noise $2qI_2$ from the charging current source, the input-referred random walk noise is

$$\overline{v_{n,I_{2c}}^2} = \left(\frac{qI_2}{C_E^2}t_c\right)\left(\frac{C_1}{C_1+C_2}\right)^2 \tag{58}$$

which is smaller than the noise during the preamplifier response time if $t_i \gg 3t_c$.

The total noise contribution from the charging current noise is then the sum of of the noise during the preamplifier response time (55) and the noise during the threshold comparator delay time (58). Assuming that the preamplifier response time dominates $t_i \gg t_c$, the charging current noise contribution is

$$\overline{v_{n,I_2}^2} \propto \frac{v_{OV}}{C_E} \tag{59}$$

where $v_{OV} = I_2 t_i/C_E$ is the fine-phase overshoot. The linearity requirement of the system determines the maximum allowed overshoot [2], [29]. Therefore, for a given linearity requirement, the charging current noise contribution is inversely proportional to the total capacitance at the output of the stage. The importance of this noise contribution increases as the capacitances used are scaled down. The charging current noise has no directly comparable source in op-amp-based designs.

3) Switch Noise: During the charge transfer phase, two switches are connected in series with the load capacitance and one in series with capacitor C_2 to the appropriate reference voltage, as shown in Fig. 17. The noise from these switches is white and results in two sources of noise for the CBSC charge transfer phase. The first source is the noise present at node v_X during the preamplifier response time. The second source is the noise present on the load capacitance at the output sampling instant. These two voltages result from the same resistor noise but are uncorrelated because they occur at different times.

The switch and capacitor network presents a white noise PSD at node v_X at the threshold detection point

$$S_{R_{\text{neq}}} = 4kTR_{\text{neq}} \tag{60}$$

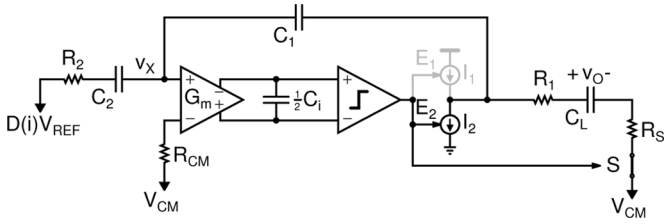

Fig. 17. Noise contribution from sampling and configuration switches.

where

$$R_{\text{neq}} = R_{CM} + (R_1 + R_S)\left(\frac{C_{1L}}{C_{1L}+C_2}\right)^2 + R_2\left(\frac{C_2}{C_{1L}+C_2}\right)^2 \tag{61}$$

and C_{1L} is the series combination of C_1 and C_L. This formulation assumes that the RC time constant of the switch and capacitor network is smaller than the preamplifier response time. The preamplifier filters the switch noise and results in jitter in the comparator decision. The transfer function to refer this noise source to the input of the stage is similar to the preamplifier response noise

$$|H_{w,\text{filter}}(f)|^2 = \left(\frac{1}{1+(2\pi f\tau_o)^2}\right)|H_{w,t_i}(f)|^2 \tag{62}$$

where $|H_{w,t_i}(f)|^2$ is defined in (43). The response for the limiting cases of preamplifier bandwidth are the same as (44a) and (44b) for the preamplifier noise, except for the factor of $1/G_m^2$.

After the preamplifier output reaches the comparator threshold, the threshold comparator trips. During the threshold comparator delay, the input no longer responds to the noise at the input of the preamplifier. Therefore, the switch and capacitor network is open loop during time $t_i \le t \le t_d$. The switch noise results in kT/C noise sampled onto the series combination of C_1, C_2, and C_L

$$\frac{1}{C_{\text{eq}}} = \frac{1}{C_1} + \frac{1}{C_2} + \frac{1}{C_L}. \tag{63}$$

The noise voltage on C_L is the kT/C noise of C_{eq} through the voltage divider from C_{eq} to the load capacitance C_L. Therefore, the input-referred noise is

$$\overline{v_{R,\text{sample}}^2} = \frac{kT}{C_{\text{eq}}}\left(\frac{C_x}{C_x+C_L}\right)^2\left(\frac{C_1}{C_1+C_2}\right)^2 \tag{64}$$

where C_x is the series combination of C_1 and C_2. Because this is a white noise source, its noise PSD is constant over the Nyquist range, and the sampled noise PSD is

$$S_{n,\text{sample}}(f) = \frac{\overline{v_{R,\text{sample}}^2}}{f_s/2}. \tag{65}$$

Note that this result could also have been obtained using the steady-state transfer function for the switch and capacitor network and the periodic filtering model.

The contribution of the filtered switched noise is similar to that in an op-amp-based implementation where the op-amp bandwidth filters the switch noise [26]. To keep this noise contribution small, the equivalent noise resistance from the switches should be lower than that of the preamplifier $R_{\text{neq}} < G_n/G_m^2$. The kT/C noise is similar to the switch noise that feeds directly to the output in an op-amp-based implementation for frequencies beyond the closed-loop bandwidth of the gain stage. Therefore, the kT/C noise places a limit on how small the capacitances can be made. Assuming a gain of two ($C_1 = C_2$) in the first stage and a load capacitance equal to half the input sampling capacitance $C_L = (C_1 + C_2)/2$, the input-referred noise contribution of the output sampling kT/C noise is only one-sixth that of the input sampler ($kT/(C_1 + C_2)$).

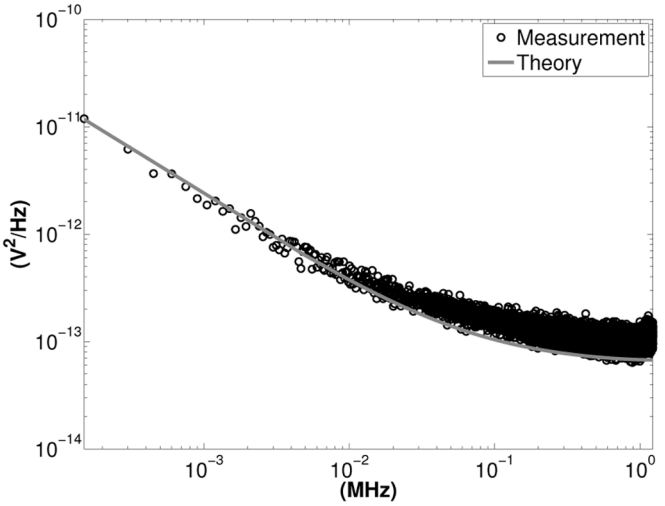

Fig. 18. Theoretical and measured noise PSD: $f_s = 2.4576$ MHz, average of 30 FFTs.

VI. Measurements

Measured results from the prototype pipeline ADC presented in [1] and [2] are compared with the analysis presented in Section V. An average periodogram estimate of the input-referred PSD of the ADC can be made from the fast Fourier transform (FFT) of several data records for a dc input to the ADC. For a sampling frequency of 2.45 MHz, both the measured and theoretical noise PSD estimates are shown in Fig. 18 on a log–log scale. The theoretical breakdown of the noise contributions is shown in Fig. 19(a), which shows that the aliased flicker noise is a significant contributor to the apparent white noise of the ADC. Fig. 19(b) shows the top-four contributors to the apparent white noise of the ADC and shows that the folded flicker noise of the preamplifier dominates, followed by the preamplifier thermal noise, the input sampler kT/C noise, and the ADC quantization noise. Table I shows a complete breakdown of all possible apparent white noise sources and their relative contributions according to the theoretical estimates obtained using the transfer functions derived in Section V. Note that the folded flicker noise and thermal noise contributions from the clamp state of the preamplifier were negligible because the desired condition of $t_i \ll \tau_o/2$ for the preamplifier was not satisfied in the prototype design.

In the prototype design, the aliased flicker noise of the input pair in the preamplifier dominates the ADC noise performance. In order to lower the flicker noise of the preamplifier, the input

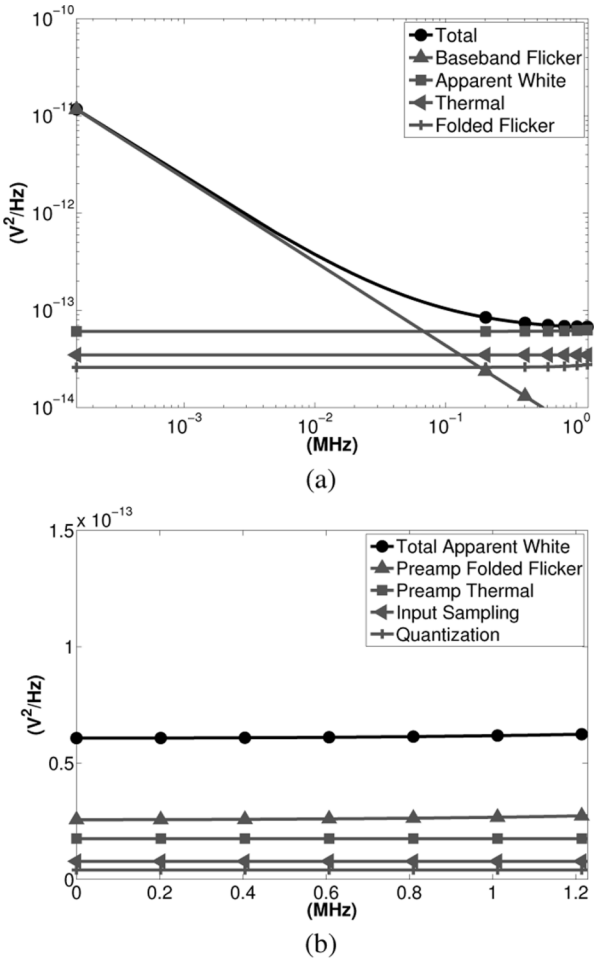

Fig. 19. Theoretical breakdown of PSD noise for $f_s = 2.4576$ MHz. (a) Theoretical breakdown of aliased components. (b) Theoretical breakdown of apparent white noise sources.

TABLE I
RANKING OF APPARENT WHITE NOISE SOURCES IN ADC PSD ESTIMATE FOR SAMPLING FREQUENCY $f_s = 2.4576$ MHz

Rank	PSD (V^2/Hz)	% of Total	Source
1	2.62×10^{-14}	42.8%	Preamp Folded Flicker
2	1.75×10^{-14}	28.6%	Preamp Thermal
3	7.79×10^{-15}	12.7%	Input Sampler
4	4.04×10^{-15}	6.60%	Quantization Noise
5	3.36×10^{-15}	5.49%	Switch Noise Preamp Response
6	1.12×10^{-15}	1.84%	Output Sample
7	7.36×10^{-16}	1.20%	Charging Current Thermal: t_c
8	2.26×10^{-16}	0.37%	Charging Current Thermal: t_i
9	1.83×10^{-16}	0.30%	Charging Current Folded Flicker: t_c
10	5.77×10^{-17}	0.09%	Charging Current Folded Flicker: t_i
11	8.46×10^{-19}	0.00%	Preamp Clamp Thermal
12	5.75×10^{-19}	0.00%	Preamp Clamp Folded Flicker

pair devices need to be made larger, since MOS device flicker noise is inversely proportional to device area [30], [31]. The input device can be made longer and wider, but the increased parasitic capacitances would require a larger bias current to maintain the same speed of operation.

VII. CONCLUSION

Circuit analysis techniques for nonstationary noise sources have been summarized and applied to the various sources of noise in a comparator-based switched-capacitor pipeline ADC. A periodic filtering model for sampling circuits was presented as an extension of existing theory for a periodic integration sampling. This method allows for the analysis of a series of output samples and the determination of an output noise PSD estimate for the system. A significant advantage of the periodic filtering approach is that it allows for the PSD analysis of both flicker and white noise sources over a series of samples using classical techniques. The periodic filtering approach was then applied to the noise analysis of the CBSC prototype pipeline ADC presented in [2], which showed a reasonable correspondence between measurement and theory. Increased flicker noise in scaled devices can lead to significant amounts of flicker noise folding if the flicker noise corner frequency is beyond the Nyquist sampling rate. In this case, folded flicker noise is a significant broadband noise contributor, as shown in Fig. 19(b). Alternatively, the sampling frequency can be made higher than the flicker noise corner frequency, and chopper stabilization or correlated double sampling can be used to remove the flicker noise.

ACKNOWLEDGMENT

The authors would like to thank National Semiconductor for providing integrated circuit fabrication and packaging. They would also like to thank J. Fiorenza for his work on the CBSC prototype pipeline ADC.

REFERENCES

[1] T. Sepke, J. K. Fiorenza, C. G. Sodini, P. Holloway, and H.-S. Lee, "Comparator-based switched-capacitor circuits for scaled CMOS technologies," in *Proc. IEEE Int. Solid-State Circuits Conf., Dig. Tech. Paper*, Feb. 2006, pp. 812–821.

[2] J. K. Fiorenza, T. Sepke, P. Holloway, C. G. Sodini, and H.-S. Lee, "Comparator based switched capacitor circuits for scaled CMOS technologies," *IEEE J. Solid-State Circuits*, vol. 41, no. 12, pp. 2658–2668, Dec. 2006.

[3] L. Brooks and H.-S. Lee, "A zero-crossing-based 8-bit 200 MS/s pipelined ADC," *IEEE J. Solid-State Circuits*, vol. 42, no. 12, pp. 2677–2687, Dec. 2007.

[4] A. Chow and H.-S. Lee, "Transient noise analysis for comparator-based switched-capacitor circuits," in *Proc. IEEE ISCAS*, May 2007, pp. 953–956.

[5] C. A. Gobet, "Spectral distribution of a sampled 1st-order lowpass filtered white noise," *Electron. Lett.*, vol. 17, no. 19, pp. 720–721, Sep. 1981.

[6] J. H. Fischer, "Noise sources and calculation techniques for switched capacitor filters," *IEEE J. Solid-State Circuits*, vol. SSC-17, no. 4, pp. 742–752, Aug. 1982.

[7] C. Enz, "Analysis of low-frequency noise reduction by autozero technique," *Electron. Lett.*, vol. 20, no. 23, pp. 959–960, Nov. 1984.

[8] H. M. Wey and W. Guggenbuehl, "Noise transfer characteristics of a correlated double sampling circuit," *IEEE Trans. Circuits Syst.*, vol. CAS-33, no. 10, pp. 1028–1030, Oct. 1986.

[9] R. Gregorian and G. C. Temes, *Analog MOS Integrated Circuits for Signal Processing*, ser. Wiley Series on Filters: Design, Manufacturing, and Applications. Hoboken, NJ: Wiley, 1986.

[10] A. Papoulis, *Probability, Random Variables, and Stochastic Processes*, 3rd ed. New York: McGraw-Hill, 1991, ch. 10 and 11.

[11] A. Leon-Garcia, *Probability and Random Processes for Electrical Engineering*, 2nd ed. Reading, MA: Addison-Wesley, 1994, ch. 6 and 7.

[12] K. K. Thornber, "Theory of noise in charge-transfer devices," *Bell Syst. Tech. J.*, vol. 53, no. 7, pp. 1211–1262, Sep. 1974.
[13] H. Tian, B. Fowler, and A. E. Gamal, "Analysis of temporal noise in CMOS photodiode active pixel sensor," *IEEE J. Solid-State Circuits*, vol. 36, no. 1, pp. 92–101, Jan. 2001.
[14] G. Xu and J. Yaun, "Performance analysis of general charge sampling," *IEEE Trans. Circuits Syst. II, Exp. Briefs*, vol. 52, no. 2, pp. 107–111, Feb. 2005.
[15] A. A. Abidi and R. G. Meyer, "Noise in relaxation oscillators," *IEEE J. Solid-State Circuits*, vol. SSC-18, no. 6, pp. 794–802, Dec. 1983.
[16] L. R. Carley and T. Mukherjee, "High-speed low-power integrating CMOS sample-and-hold amplifier architecture," in *Proc. IEEE Custom Integr. Circuits Conf.*, 1995, pp. 543–546.
[17] G. Xu and J. Yuan, "Comparison of charge sampling and voltage sampling," in *Proc. 43rd IEEE Midwest Symp. Circuits Syst.*, Aug. 2000, pp. 440–443.
[18] S. Kaworten, T. Riley, and J. Kostamovanra, "A low noise quadrature subsampling mixer," in *Proc. IEEE Int. Symp. Circuits Syst.*, 2001, pp. 790–793.
[19] S. Karvonen, T. A. D. Riley, and J. Kostamovaara, "A CMOS quadrature charge-domain sampling circuit with 66-dB SFDR up to 100 MHz," *IEEE Trans. Circuits Syst. II, Exp. Briefs*, vol. 52, no. 2, pp. 292–304, Feb. 2005.
[20] K. Muhammad and R. B. Staszewski, "Direct RF sampling mixer with recursive filtering in charge domain," in *Proc. IEEE Int. Symp. Circuits Syst.*, 2004, pp. 577–580.
[21] A. A. Abidi, "Phase noise and jitter in CMOS ring oscillators," *IEEE J. Solid-State Circuits*, vol. 41, no. 8, pp. 1803–1816, Aug. 2006.
[22] M. S. Keshner, "Renewal process and diffusion models of $1/f$ noise," Ph.D., MIT, Cambridge, MA, 1979.
[23] N. J. Kasdin, "Discrete simulation of colored noise and stochastic processes and $1/f^{\alpha}$ power law noise generation," *Proc. IEEE*, vol. 83, no. 5, pp. 802–827, May 1995.
[24] J. Phillips and K. Kundert, "Noise in mixers, oscillators, samplers, and logic: An introduction to cyclostationary noise," in *Proc. IEEE Custom Integr. Circuits Conf.*, 2000, pp. 431–438.
[25] B. J. McCarroll, C. G. Sodini, and H.-S. Lee, "A high-speed CMOS comparator for use in an ADC," *IEEE J. Solid-State Circuits*, vol. 23, no. 1, pp. 159–165, Feb. 1988.
[26] T. Sepke, "Comparator design and analysis for comparator-based switched-capacitor circuits," Ph.D., MIT, Cambridge, MA, 2006.
[27] B. Ginetti and P. G. A. J. Vandemeulebroecke, "A CMOS 13-b cyclic RSD A/D converter," *IEEE J. Solid-State Circuits*, vol. 27, no. 7, pp. 957–965, Jul. 1992.
[28] H.-S. Lee, "A 12-b 600 ks/s digitally self-calibrated pipelined algorithmic ADC," *IEEE J. Solid-State Circuits*, vol. 29, no. 4, pp. 509–515, Apr. 1994.
[29] J. K. Fiorenza, "A comparator-based switched capacitor pipelined analog-to-digital converter," Ph.D., MIT, Cambridge, MA, 2007.
[30] S. Christensson, I. Lundstroem, and C. Svensson, "Low frequency noise in MOS transistors–I Theory," *Solid State Electron.*, vol. 11, no. 9, pp. 797–797, Sep. 1968.
[31] A. van der Ziel, "Dependence of flicker noise in MOSFETs on geometry," *Solid State Electron.*, vol. 20, no. 3, pp. 267–267, Mar. 1977.

Todd Sepke (S'01–M'07) was born in Detroit, MI, in 1975. He received the B.S.E.E. degree from Michigan State University, East Lansing, in 1997 and the M.S. and Ph.D. degrees in electrical engineering from the Massachusetts Institute of Technology, Cambridge, in 2002 and 2006, respectively.

He is currently with Marvell Semiconductor, Inc., Santa Clara, CA. His research interests include RF, analog, and mixed-signal circuit design.

Peter Holloway is currently with National Semiconductor, Salem, NH.

Charles G. Sodini (S'80–M'82–SM'90–F'94) received the B.S.E.E. degree from Purdue University, West Lafayette, IN, in 1974 and the M.S.E.E. and Ph.D. degrees from the University of California, Berkeley, in 1981 and 1982, respectively.

He was a Member of the Technical Staff with Hewlett–Packard Laboratories from 1974 to 1982, where he worked on the design of MOS memory. He joined the faculty of the Massachusetts Institute of Technology, Cambridge, in 1983, where he is currently the LeBel Professor of Electrical Engineering. His research interests are focused on mixed-signal integrated circuit and system design. Along with Prof. R. T. Howe, he is the coauthor of an undergraduate textbook on integrated circuits and devices entitled, *Microelectronics: An Integrated Approach* (Prentice-Hall, 1997). He was a cofounder of SMaL Camera Technologies, a leader in imaging technology for consumer digital still cameras and machine vision cameras for automotive applications.

Dr. Sodini has served on a variety of IEEE conference committees, including the International Electron Device Meeting, where he was the 1989 General Chairman. He has served on the IEEE Electron Device Society Administrative Committee and was President of the IEEE Solid-State Circuits Society from 2002 to 2004. He is currently the chair of the Executive Committee for the VLSI Symposia.

Hae-Seung Lee (M'85–SM'92–F'96) received the B.S. and M.S. degrees in electronic engineering from Seoul National University, Seoul, Korea, in 1978 and 1980, respectively, and the Ph.D. degree in electrical engineering from the University of California, Berkeley, in 1984, where he developed self-calibration techniques for analog-to-digital (A/D) converters.

Since 1984, he has been on the faculty of the Department of Electrical Engineering and Computer Science, Massachusetts Institute of Technology (MIT), Cambridge, where he is currently a Professor and the Director of the Center for Integrated Circuits and Systems. From 1985 to 1999, he acted as a consultant to Analog Devices, Inc., Wilmington, MA, and MIT Lincoln Laboratories. He is on the Technology Advisory Board for Sensata Technologies and served the Technology Advisory Committee for Samsung Electronics and Cypress Semiconductor from 2004 to 2007 and from 2005 to 2007, respectively. In 1999, he cofounded SMaL Camera Technologies, which was later acquired by Cypress Semiconductor in 2005. His research interests are in the areas of analog integrated circuits with an emphasis on A/D converters in scaled CMOS technologies.

Prof. Lee was a recipient of the 1988 Presidential Young Investigators' Award and a corecipient of the ISSCC Jack Kilby Outstanding Student Paper Award in 2002 and 2006. He has served a number of technical program committees for various IEEE conferences, including the International Electron Devices Meeting, the International Solid-State Circuits Conference, the Custom Integrated Circuits Conference, and the IEEE Symposium on VLSI Circuits. He is an elected AdCom member of the Solid-State Circuits Society.